Commissioning of a high-resolution collinear laser spectroscopy apparatus using a laser ablation ion source*

Shi-Wei Bai,[1] Xiao-Fei Yang,[1,†] Shu-Jing Wang,[1] Yong-Chao Liu,[1] Peng Zhang,[1] Yin-Shen Liu,[1] Han-Rui Hu,[1] Yang-Fan Guo,[1] Jin Wang,[1] Ze-Yu Du,[1] Zhou Yan,[1] Yun-kai Zhang,[1] Yan-Lin Ye,[1] Qi-Te Li,[1] Yu-Cheng Ge,[1] and Chuang-Ye He[2]

[1]*School of Physics and State Key Laboratory of Nuclear Physics and Technology, Peking University, Beijing 100871, China*
[2]*China Institute of Atomic Energy (CIAE), P.O. Box 275(10), Beijing 102413, China*

Collinear laser spectroscopy is known as one of the powerful tools for the study of nuclear spins, electromagnetic moments and charge radii of the exotic nuclei. Aiming at studying these nuclear properties of unstable nuclei at the Beijing Radioactive Ion-beam Facility (BRIF) and the future High Intensity Heavy-ion Accelerator Facility (HIAF), we have firstly developed a collinear laser spectroscopy apparatus integrated with an offline laser ablation ion source and a laser system. The overall performances of this state-of-the-art technique and device have been commissioned by using the bunched stable ion beam. High-resolution optical spectra of ^{40,42,44,48}Ca isotopes were successfully measured for the $4s\ ^2S_{1/2} \rightarrow 4p\ ^2P_{3/2}$ (D2) ionic transition and the extracted isotope shifts relative to the ^{40}Ca show an excellent agreement with the literature values. This system is now ready to be applied at the ratioactive ion beam facility, such as BRIF, and has paved the way for further development of the higher-sensitivity collinear resonant ionization spectroscopy.

Keywords: Nuclear properties, Collinear laser spectroscopy, Laser-ablation ion source, Photon detection, Isotope shift

I. INTRODUCTION

Understanding the nuclear structural evolution of short-lived exotic nuclei towards the proton and neutron driplines is one of the main topics in the current nuclear physics research, triggering continuous developments of experimental techniques and theoretical approaches [1, 2]. The static properties of the ground and isomeric states of unstable nuclei are of indispensible importance for the study of exotic nuclear structure [3–5], and also represent a stringent test of the different nuclear models [6, 7]. Collinear laser spectroscopy (CLS) has been proven to be one of the powerful tools to access multiple nuclear properties of the ground and isomeric states of exotic nuclei [8, 9]. This is realized by probing the hyperfine structure (hfs) and isotope shift resulted from the interaction between the atomic nucleus and surrounding electrons, which allow to precisely extract the nuclear spins (I), magnetic dipole moments (μ), electric quadrupole moments (Q_s), and changes in the mean square charge radii ($\delta \langle r^2 \rangle$) of an isotopic chain in a nuclear model-independent way.

Along with the observation of unexpected nuclear phenomena in short-lived exotic nuclei, the upgrade of existing and the development of next-generation radioactive ion beam (RIB) facilities are motivated with the aim to produce more exotic radioactive beams. Meanwhile, considerable efforts have been made to continuously enhance the experimental sensitivity and precision of the CLS method [10, 11], facilitating the unceasing studies of exotic nuclei. Up to now, this experimental technique has been established at different RIB facilities, e.g. ISOLDE/CERN [12], IGISOL/JYFL [13], ISAC/TRIUMF [14], NSCL/MSU [15] and ALTO [16], yielding major inputs for nuclear structure study and providing important benchmark for the development of state-of-the-art nuclear theory [7, 17–19].

Two operational RIB facilities are available in China, i.e. HIRFL (PF-type) at IMP of Lanzhou [20] and BRIF (ISOL-type) at CIAE of Beijing [21], which have played a significant role in the nuclear physics research [20–22]. To gain access to more rare isotopes, two next generation RIB facilities, high intensity heavy ion accelerator facility (HIAF) [23] and beijing isotope-separation-on-line neutron-rich beam facility (BISOL) [24] are under construction and planned, respectively, offering new opportunities for nuclear physics studies in the near future. However, the well-established CLS technique has so far not been implemented at these domestic RIB facilities. Therefore, in order to take the full advantages of the short-lived isotopes available at these RIB facilities, we have, as a first stage, developed a CLS device combined with an offline laser ablation ion source in order to fully master the laser spectroscopy technique for nuclear properties measurement. This integrated system also paves the way for the further development of high-sensitivity collinear resonance ionization spectroscopy, which allows for the exploration of the more exotic cases.

Here, we present the details of the newly developed CLS apparatus, including the laser ablation ion source with up to 30 keV HV platform, the beamline with the photo detection system, the laser system, and data acquisition system. Thanks to the ion bunches (with about 10 μs temporal length) offered by the laser ablation ion source, the first commissioning experiment was successfully performed to probe the $4s\ ^2S_{1/2} \rightarrow 4p\ ^2P_{3/2}$ (D2) ionic transition of calcium. High-resolution optical spectra of four stable ^{40,42,44,48}Ca isotopes were measured, reaching a typical linewidth of $\sim$55 MHz, being comparable with the well-established standard CLS setup worldwide [6, 15, 25]. Isotope shifts ($\delta\nu^{40,A}$) of ^{42,44,48}Ca isotopes relative to ^{40}Ca reference isotope were extracted, which are

* This work was supported by the National Natural Science Foundation of China (Nos. 12027809, U1967201, 11875073, 11875074 and 11961141003), National Key R&D Program of China (No. 2018YFA0404403), China National Nuclear Corporation (No. FA18000201), and the State Key Laboratory of Nuclear Physics and Technology, Peking University (No. NPT2019ZZ02).

† Corresponding author xiaofei.yang@pku.edu.cn

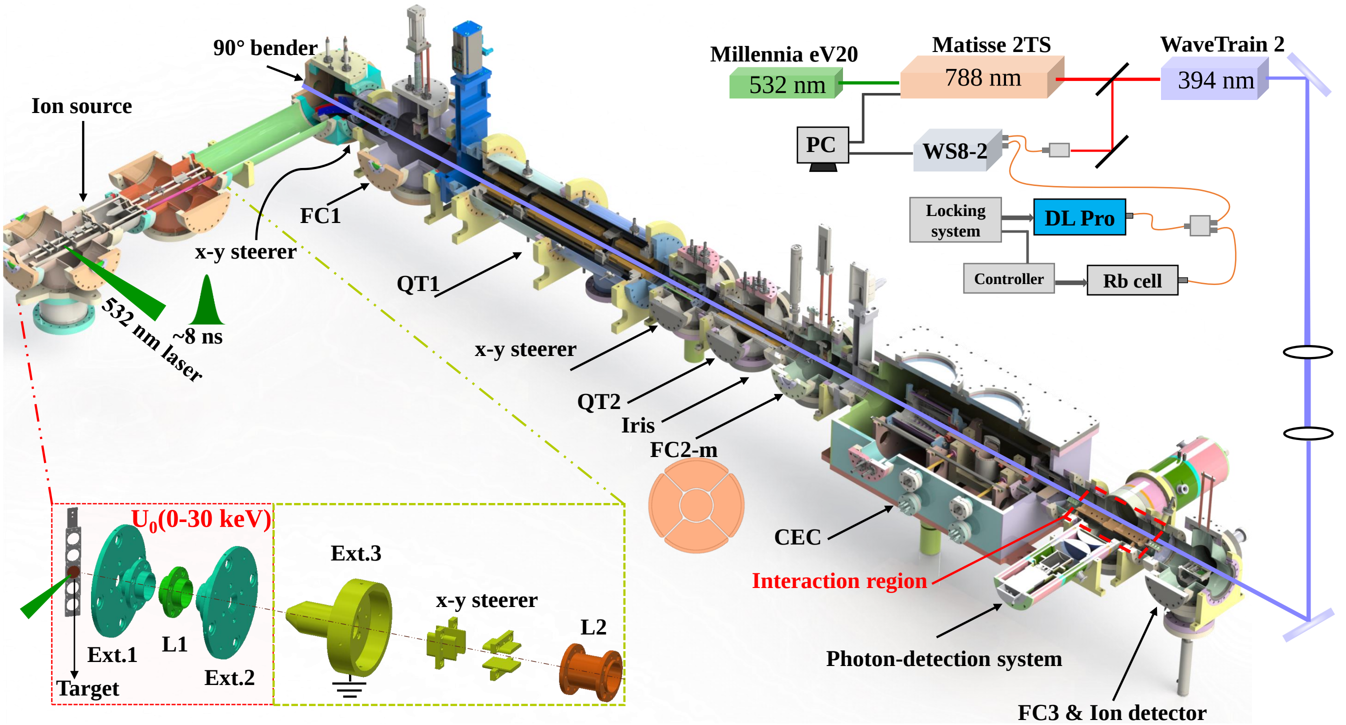

Fig. 1. Schematic view of the CLS device, the electrodes of laser ablation ion source (bottom left inset) and the adopted laser system (top right inset). The stable ion bunches with up to 30 keV energy can be delivered into the beamline, and overlapped with a continuous-wave frequency tunable laser beam in an anti-collinear geometry. The ion beam velocity or laser frequency is tuned to resonantly excite the ions in the interaction zone. The fluorescence photons emitted from the excited ions are collected by the photon detection system. See text for more details.

in excellent agreement with the literature values [6, 26, 27].

II. COLLINEAR LASER SPECTROSCOPY SYSTEM

Figure 1 presents a detailed sketch of the CLS apparatus, laser ablation ion source and the laser system. The whole setup is constructed according to the ConFlat (CF) standard for a high vacuum condition, which is currently $\sim 10^{-8}$ mbar, permitting a subsequent upgrade of high-sensitivity collinear resonance ionization spectroscopy setup. With the current system, the hfs spectra of the stable ion beams produced by the ion source can be measured with high-resolution. In brief, the bunched ion beam extracted from the laser ablation target (solid material) is accelerated up to 30 keV. After a 90° electrostatical deflection, the ion bunch is delivered into the CLS beamline, where it is anti-collinearly overlapped with a continuous wave (cw) laser beam. The velocity of the ions can be tuned by applying a scanning voltage to the electrode in the interaction region. The fluorescence photons emitted from the laser excited ions are collected and recorded by the photon detection system and data acquisition system, as a function of the tuning voltage. In the case of probing a transition from neutral atoms, a charge exchange cell (CEC, see Fig. 1) will be required, and the scanning voltage will be applied to an electrode upstream of the CEC. This part will however not be introduced here as we will focus mainly on the Ca ion beam measurement. The functional details of the individual parts will be introduced in the following sections.

A. Laser ablation ion source

The laser ablation ion source is developed to produce stable ion beams of a wide range of elements with an energy of up to 30 keV [25, 28]. By using a pulsed-laser ablation process, bunched ion beams with a typical temporal length of about 10 μs, a high ion intensity and a low energy spread can be generated. These features of the ion beam are suitable for the optimization and commissioning of the system of CLS and future resonance ionization spectroscopy, for the development laser excitation and ionization schemes [28], and for the measurement of atomic hfs parameters of stable isotopes [29].

The inner structure of the ion source is shown schematically in Fig. 1 (left bottom inset). A 532-nm Nd: YAG laser (Litron TRLi 250-100), operated at 100 Hz repetition rate and with a pulse width of $\sim$8 ns, is employed for the ablation of the solid target. The target holder, floated at the acceleration (platform) potential (U_0: up to 30 keV) is tilted at 45° with respect to the laser beam and ion beam. The pulsed laser beam is focused onto the target material with a diameter of approximately 1 mm. The ions generated at the ablation area are extracted and refocused with a multiple-step extraction system, namely the first extraction electrode (Ext.1), the first einzel lens (L1) and the second extraction electrode (Ext.2).

A negative potential (up to 6 keV) relative to the platform potential U_0 can be applied independently to these electrodes. The extracted ions are then transported to the third extraction electrode (Ext.3) at ground potential, and are simultaneously accelerated to a final energy of up to 30 keV. Before being directed into the CLS beamline by a pair of 90° bender plates, the accelerated ion beam transportation can be further corrected by a group of horizontal- and vertical-steerers and by the second einzel lens (L2).

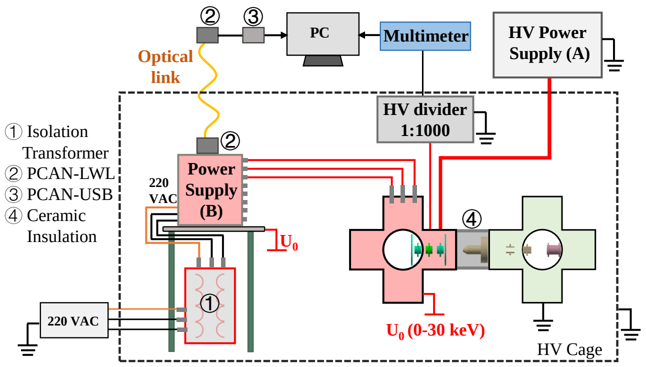

Fig. 2. Schematic diagram of the high voltage system applied for laser ablation ion source, which can be operated at 0-30 keV.

As above mentioned, the voltages applied to the electrodes (Ext.1, L1 and Ext.2) are floated on the top of acceleration potential U_0. Therefore, as shown in Fig. 2, a high-voltage (HV) platform and a HV cage (indicated with dashed line) are built, following the guidelines for safety practices. The acceleration potential U_0 is provided by a high-precision DC power supply (Heinzinger PNChp 40000-15pos) with a ripple of $<0.001\%$ and a long-term stability of $<0.001\%$ over 8 hours. This U_0 potential is directly applied to the first CF 6-Way cross chamber (light red part in Fig. 2) of the ion source, which is fully isolated from the second 6-Way cross at ground potential (light green part in Fig. 2) by a CF flanged vacuum ceramic break. A multichannel HV power supply module (iseg EHS 80-60n) installed in a HV crate (iseg ECH224), marked as power supply B, is used to control the negative potential of the three electrodes (Ext.1, L1 and Ext.2) inside of the first 6-Way Cross. The power supply B is remotely controlled outside the HV cage via an optical link (PEAK-System Technik, PCAN-LWL) for HV isolation and a USB adapter (PEAK-System Technik,PCAN-USB). An isolation transformer (50 kV) is used to isolate the high voltage (U_0) from the ground potential and provide the 220 VAC to the power supply B. To determine the energy of the ion beam for the hfs measurement, the acceleration potential U_0 is recorded in real time using a keysight 34470A multimeter combined with a 1:1000 voltage divider (Ohm-labs, KV-30A).

B. Ion beam transport

The ion bunches are transported through the CLS beamline (about 4 meters long) using a serials of electrostatic optics elements, including two sets of x-y steerers and two quadrupole triplet (QT1 and QT2) lens, as shown in Fig. 1. The x-y steerer electrodes are used to align the ion beam with the central axis of the beamline, and QT lenses to control the beam spot. Ion beam diagnostic components, consisted of three Faraday cups (FC1, FC2-m and FC3) with a secondary-electron suppressor, one iris diaphragm and one ion detector (ETP, 14924 MagneTOF Mini), are used to monitor the beam position, intensity and size. The iris diaphragm with a tunable diameter of 0-20 mm is placed in front of the FC2-m (a multi-channel FC) to align the central axis of ion and laser beams, which can also serves as a simple annular FC to measure the ion beam current and size [30]. The FC ion beam current is recorded by a Keithley 6485 picoammeter. The potentials applied to the ion optics are provided by the $\pm$ 6 kV HV modules combined with a HV crate (iseg ECH238). Using a program written in Python, the output voltage of the HV power supplies can be remotely controlled. The program is also used for visualizing the ion beam current. Therefore, an optimization of the ion beam transmission through the CLS beamline can be achieved remotely. The magneTOF ion detector installed at the end of the beamline is used to assess the intensity and the time of flight (TOF) of a weak ion beams.

C. Photon detection system

Figure 3 presents the schematic diagram of the photon-detection system. The system consists of a 5-way-cross interaction chamber in which the laser beam interacts with the atom/ion beam, and two identical detection units installed perpendicularly to the CLS beamline. To suppress the environmental photon background, i.e. the scattered laser light, the interaction chamber is equipped with two dis-mountable arrays of tapered apertures, each having an inner diameter of 10 mm, as indicated in Fig. 3(a). The internal surface of the vacuum chamber is black-coated in order to further reduce the background from laser scattering. A quartz window (VPZL-600 DU, Kurt J. Lester) with >90% transmission for a wide spectrum range of 200-1200 nm is adopted to isolate the detection units from the high-vacuum interaction region at $\sim 10^{-8}$ mbar. Note that an isolated electrode tube is mounted in the central axis of the interaction chamber, with two open rectangular holes in the direction of the detection unit for the fluorescence photon transmission. To maintain an uniform field distribution inside of the electrode tube (interaction region), the holes are covered with a metallic mesh with a transmission efficiency higher than 90%. By applying a scanning voltage to this electrode, the velocity of the ions (not applicable to neutral atoms) can be tuned to match with the Doppler-shifted laser frequency for the specific resonant excitation (see Sec. III for details).

As shown in Fig. 3, each detection unit is composed of two aspheric lenses (namely a telescope), and a PMT. These lenses, with a diameter of 100 mm (N-BK7), have a transmitivity of $\sim$90% over a wide range of wavelength 350-1000 nm, which are used to guide the laser-induced fluorescence photons onto the sensitive area of the PMT. A PMT (R943-02, Hamamatsu) assembled with a socket (E2762-506

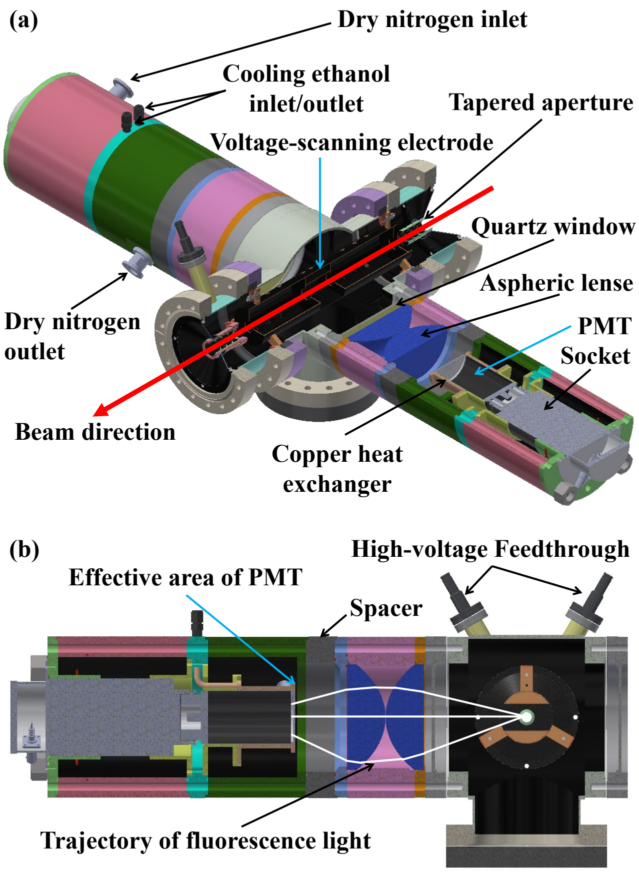

Fig. 3. (a) Photon detection system consisting of two sets of detection units, each including a quartz window, two aspheric lens and a photon-multiplier tube [31]. (b) A schematic view of one detection unit.

Hamamatsu) is employed to record the light. This PMT is featured with the ultra low dark count rate (typical 20 s^{-1} at $-20°$C) and the wide spectral response (160-930 nm), but with a moderate sensitive area of 10×10 mm^2. The quantum efficiency of this PMT at 394 nm is $\sim$20%. Using two detection units, a total geometrical efficiency for fluorescence photon is simulated to be $\sim$15% [32]. The distance between the lens and the PMT is adjustable, which is realized by changing the thickness of the spacer (e.g. 27.3 mm for a wavelength of 394 nm), in order to ensure an optimal geometrical efficiency for various wavelength associated with specific ionic/atomic transitions.

To reach a low dark count rate (dozens of counts per second), the R943-02 PMT needs to be maintained at the temperature of $-20 - -30°$C. To cool the GaAs (Cs) photocathode, the head of the PMT is covered by a spiral copper tube, named as copper heat exchanger in Fig. 3, through which the ethanol is circulated by a refrigerant circulator (ECO RE 630S, LAUDA). In order to prevent the formation of the frost/ice in the glass window of the PMTs resulted from the low-temperature environment, the dry nitrogen gas is circulated in the system for few minutes before cooling. The above-mentioned spacer, made of PVC, is also used as a thermal isolation between the PMT and lens, which can effectively avoid the damage of the lens due to the expansion and contraction caused by temperature variation. Based on all these treatments, the achieved typical background rate is about 1 kHz for a 1.2-mW laser beam (about 6-mm diameter). It is worth mentioning that the whole detection unit (include the PMT) is proved to be robust and stable after frequent assembly and disassembly during the commissioning.

D. Laser system

The laser system used for this CLS setup is partly shown in the top right inset of Fig. 1. The continuous-wave (cw) titanium-sapphire (Ti:Sa) laser (Matisse 2TS, Sirah Lasertechnik) is pumped by a 20 W 532 nm laser (Millennia, Spectra-Physics), which can also be converted into the Dye system via an Exchange Kit (TIDYECW, Sirah Lasertechnik). This system provides a laser beam with a wavelength range of 650-1020 nm, which can be further frequency-doubled with the Wavetrain 2 (Sirah Lasertechnik), generating the 2$^{\rm nd}$ harmonic light covering the wavelength range of 325-500 nm. The Matisse cavity can be actively stabilized by the equipped reference cell, reaching a narrow linewidth of $<$ 50 kHz. A high-precision wavelength meter (HighFinesse WS8-2) is used to measure the real-time frequency of the fundamental cw light.

The wavelength meter can also be used to perform a long-term stabilization of Matisse cavity through a built-in digital interface. To address the drift problem of the wavelength meter (about several MHz per day), caused by temperature and pressure fluctuations, a commercial saturation absorption spectroscopy unit is introduced. This unit consists of a tunable Diode laser (DLPRO780, TOPTICA Photonics AG), a temperature controlled vapor cell filled with K, Rb, and Cs (COSY), as well as the control and locking electronics. The frequency of diode laser is locked to one of the hyperfine components of the available alkali atom (e.g. ^{87}Rb). The frequency-locked diode laser is then used to calibrate the wavelength meter when it functions as a long-term stabilization of the Matisse [33], or to correct the drift of the wavelength meter by recording both frequency-scanned Matisse laser and frequency-locked Diode laser [34].

E. Electronics and data acquisition system

Two signals from the PMTs are amplified by a fast-timing amplifier (ORTEC FTA820A) and then discriminated by a constant fraction discriminator (CFD, CAEN model N605). After converting to TTL logic signals, they are sent to different channels of a ChronoLogic TimeTagger4-2G time-to-digital converter (TDC) with a 500 ps time resolution. Each event labeled by a timestamp could be tracked to obtain the time of flight (TOF) spectrum of the ion bunch. A master TTL signal with 100 Hz repetition rate (a period of 10 ms), labeled as $T_0 = 0$ μs and generated by a Quantum Composers 9528 (QC9528) digital-delay pulse generator, is used to externally

trigger the 532-nm Nd: YAG laser. The laser pulse used for the ablation ion sources arrives 490 μs later than T_0. Therefore, after taking into account of the flight time of the ion bunch from the ion source to the detection region, the start time (trigger) and the time window for the TDC are set to be $\mathrm{T}_1 = \mathrm{T}_0 + 498\ \mu$s and $\Delta\mathrm{T} = 100\ \mu$s, respectively. This time widow covers the time period when the bunched beam is traversing the photon detection region. A narrow time gate, $\sim$10 μs corresponding to the width of the ion bunch, can be further applied to reduce the background counts during the offline analysis (more discussion in Sec. III).

The optical hfs spectrum of an isotope is measured by applying a scanned voltage (ΔU) to the electrode tube in the interaction detection region, while the laser frequency is fixed and stabilized with the wavelength meter. A scanned voltage between -1 keV and $+1$ keV can be provided by a DC amplifier (Kepco Model BOP 1000DM) with a gain of 100 and a long-term stability of $< 0.01\%$ over 8 hours, which is controlled by a USB device (USB-3106, Measurement Computing). A real-time measurement of the ΔU applied to the electrode tube and the starting potential U_0 of the ion beam are realized by a Keysight 34470A digital multimeter.

A program written in Python is used for the acquisition system. This program integrates the functions of logging the photon events from the TDC, controlling the scanning voltage via the USB device, recording the frequencies of Matisse and Diode laser via the wavelength meter, reading the scanned voltage and starting potential of the ions through the multimeter, as well as the display of the results via the graphical interface.

III. COMMISSIONING TEST AND RESULTS

To validate the performance of the CLS system, we performed the first commission experiment on natural ^{40,42,44,48}Ca isotopes by probing the $4s\ ^2S_{1/2} \rightarrow 4p\ ^2P_{3/2}$ (D2) ionic transition. The stable beams were produced by ablating a calcium target using the 532 nm laser (about 1 mm beam diameter on the target) with an approximately 1.5 mJ/pulse power. In this test experiment, the extracted ion bunches were accelerated to 20 keV and delivered to the CLS beamline. The ion beam was anti-collinearly overlapped with the frequency-fixed cw laser beam (Fig. 1). The laser frequency was stabilized by the wavelength meter, which was calibrated by the diode laser locked to one hyperfine component of the ^{87}Rb atom. The used laser power is about 1.2 mW, and the diameter of the laser spot is $\sim$6 mm. The velocity of Ca ion was tuned in the interaction region by applying a scanning voltage (ΔU) to the electrode tube (Fig. 3). As a result, in the anti-collinear configuration, the Dopper-shifted laser frequency ν experienced by the calcium ion beam can be calculated in the rest frame as:

$$\nu = \nu_0 \times \frac{\sqrt{1-\beta^2}}{1-\beta} \tag{1}$$

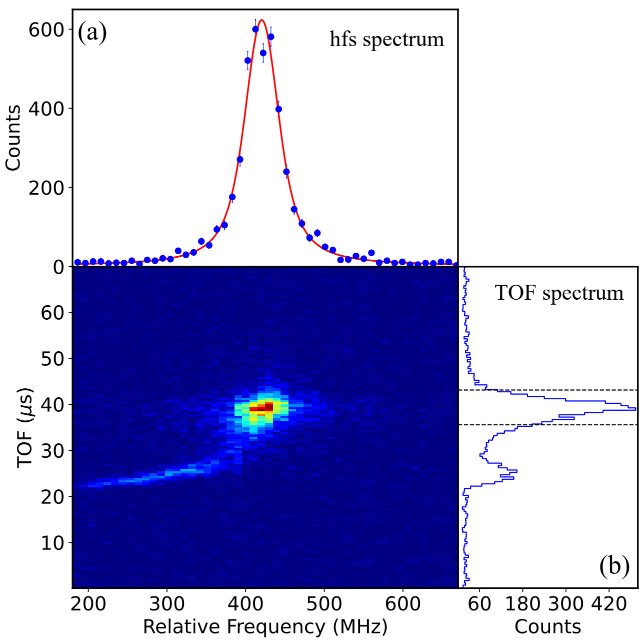

Fig. 4. Color-coded two-dimensional spectrum, TOF vs frequency, for ^{40}Ca$^+$. The projection of this plot onto x-axis (relative laser frequency) and y-axis (time of flight: TOF) leads to the hfs spectrum (a) and TOF spectrum (b). A typical temporal gate of $\sim$10 μs, as indicated by the dotted lines in (b), is applied to obtained the hfs spectrum as displayed in (a). The hfs spectrum is fitted with a Voigt line profile (red line).

with

$$\beta = \sqrt{1 - \frac{m^2c^4}{(eU + mc^2)^2}} \tag{2}$$

where ν_0 is the fixed laser frequency, U is the total potential ($U = U_0 + \Delta U$) and m is the mass of the Ca ion. By counting the emitted fluorescence photons from the resonantly excited ions as a function of the tuning voltage (ΔU), the optical spectra for Ca isotopes were obtained.

Figure 4 presents a typical two-dimensional spectrum for relative laser frequency and TOF. The projection of the photon counts onto the x-axis and y axis lead to the hfs spectrum (Fig. 4(a)) and TOF spectrum (Fig. 4(b)), respectively. The typical temporal length of the ion bunch is about 10 μs, but with a visible tail in the higher energy side (the shorter TOF side), as shown in the TOF spectrum. Such higher energy tail is related to the field distribution within the plasma plume of the ablation process, as described in Refs. [25, 28]. A TOF correction method [28, 29] can be applied to compensate the higher energy component of the ion bunches, which leads to the similar result as that achieved by simply gating on the main TOF peak, as indicated by the dotted lines in TOF spectrum. This low probability tail is nearly invisible when a weak ion beam is adopted, e.g. the ion beam current of < 1 pA as that for ^{42,44,48}Ca.

The high-resolution hfs spectra of ^{40,42,44,48}Ca, obtained by gating the TOF window as indicated in Fig. 4(b), are shown in the insets of Fig. 5, which are fitted using a Voigt

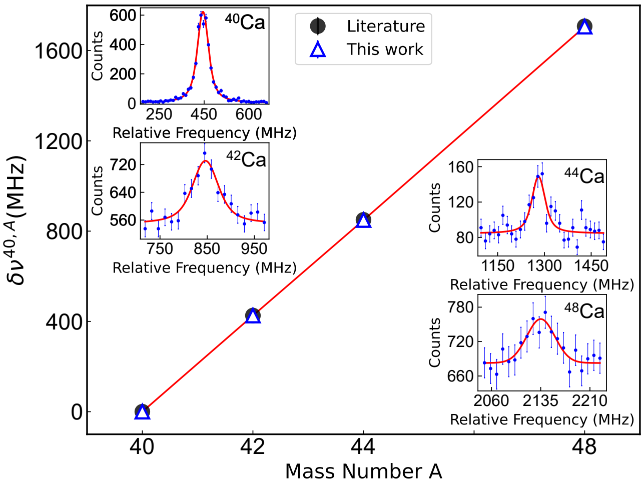

Fig. 5. Presently measured isotopes shifts of ^{40,42,44,48}Ca for the $4s\ ^2S_{1/2} \rightarrow 4p\ ^2P_{3/2}$ (D2) ionic transition in comparison to literature values [26]. The optical spectra for ^{40,42,44,48}Ca shown in the insets are fitted with Voigt line profiles (red lines).

TABLE 1. Isotope shifts (in MHz) of ^{42,44,48}Ca isotopes relative to ^{40}Ca measured for the $4s\ ^2\mathrm{S}_{1/2} \rightarrow 4p\ ^2\mathrm{P}_{3/2}$ (D2) ionic transition. These results are compared with the literature values [26, 27]. Note that the isotope shifts from Ref. [27] are from a dedicated experimental setup for high-precision measurement.

	This work	Ref. [26]	Ref. [27]
40	-	-	-
42	426.9(29)	426.4(15)(10)	426.04(15)
44	848.8(37)	850.1(10)(19)	850.09(14)
48	1705.7(39)	1710.6(35)(39)	1707.58(16)

profile (a convolution of Gaussian and Lorenzian). The full width at half maximum (FWHM) of the spectra from the Voigt fit is about 55 MHz, which is comparable to the same type of CLS measurements worldwide [6, 15, 25]. Considering the natural line width of about 25 MHz (main contribution for the Lorenzian component Γ_L) for the $4s\ ^2S_{1/2} \rightarrow 4p\ ^2P_{3/2}$ (D2) ionic transition, the maximal Gaussian contribution (Γ_G) of the FWHM is about 40 MHz, which is mainly attributed to the energy spread of the ion beam. Assuming an energy spread δE for the total potential U of ion beam, the resulted Doppler broadening of the spectral line will be:

$$\delta\nu = \nu_0 \times \frac{\delta E}{\sqrt{2eUmc^2}}. \tag{3}$$

Thus, the ∼40 MHz Gaussian (Γ_G) contribution in linewidth corresponds to an energy spread of ∼2 eV for the ion beam, which is mainly attributed to the fluctuation of the Heinzinger power supply (∼200 mV: 4 MHz), Kepco DC amplifier (∼ 20 mV) and the field distribution at the position of the ablation target. From these high-resolution optical spectra (shown in the insets of Fig. 5), isotope shifts of ^{42,44,48}Ca$^+$ relative to reference isotope ^{40}Ca$^+$ are extracted, which are in good agreement with the literature values [26, 27], as displayed in Fig. 5 and summarized in Table 1.

IV. SUMMARY AND PROSPECTS

In summary, a collinear laser spectroscopy apparatus integrated with a laser ablation ion source and a frequency tunable laser system, have been implemented at Peking University, aiming at studying nuclear properties of unstable nuclei at the domestic RIB facilities. The ion source was designed to provide the bunched stable ion beam with a beam energy up to 30 keV, which was commissioned with the 20 keV bunched stable calcium ion beam. The typical temporal width of the ion bunch was determined to be about 10 μs. Combined with an anti-collinear laser of 394 nm, high resolution hfs spectra were measured for stable ^{40,42,44,48}Ca isotopes, reaching a narrow linewidth of about 55 MHz (FWHM), which is comparable to the same type of CLS setups worldwide. The Gaussian component of the linewidth (FWHM) was determined to be about 40 MHz, corresponding to an energy spread of ∼ 2 eV for the stable calcium ion beam. Isotope shifts ($\delta\nu^{40,A}$) of ^{42,44,48}Ca relative to the reference ^{40}Ca$^+$, extracted from the obtained hfs spectra, are in excellent agreement with the literature, demonstrating the overall satisfactory performance of this CLS system.

Based on the successful implementation and operation, the entire system is now ready to be applied to study unstable isotopes at the RIB facilities, such as BRIF of CIAE. This kind of online experiment is scheduled and will be performed in a short term. In addition, further exploration and developments of the CLS technique are also planned in the coming steps, e.g. the application of system for atomic hfs spectrum measurement using a charge exchange process and the development of the system towards a resonant ionization spectroscopy measurement. A mass separator and a radio-frequency quadrupole cooler/buncher can also be incorporated into the system, in order to provide ion beam bunch with a better time structure.

[1] T. Otsuka, A. Gade, O. Sorlin et al., Evolution of shell structure in exotic nuclei. Rev. Mod. Phys. **92**, 015002 (2020). https://doi.org/10.1103/RevModPhys.92.015002

[2] F. Nowacki, A. Obertelli and A. Poves, The neutron-rich edge of the nuclear landscape: Experiment and theory. Progress in Particle and Nuclear Physics. **120**, 103866 (2021).

https://doi.org/10.1016/j.ppnp.2021.103866

[3] W. Nörtershäuser, D. Tiedemann, M. Žáková et al., Nuclear Charge Radii of ^{7,9,10}Be and the One-Neutron Halo Nucleus ^{11}Be. Phys. Rev. Lett. **102**, 062503 (2009). doi/10.1103/PhysRevLett.102.062503

[4] K.T. Flanagan, P. Vingerhoets, M. Avgoulea et al., Nuclear Spins and Magnetic Moments of ^{71,73,75}Cu: Inversion of $\pi 2p_{3/2}$ and $\pi 2f_{5/2}$ Levels in ^{75}Cu. Phys. Rev. Lett. **103**, 142501 (2009). 10.1103/PhysRevLett.103.142501

[5] X. F. Yang, C. Wraith, L. Xie et al., Isomer Shift and Magnetic Moment of the Long-Lived $1/2^+$ Isomer in $^{79}_{30}$Zn$_{49}$: Signature of Shape Coexistence near ^{78}Ni. Phys. Rev. Lett. **116**, 182502 (2016). doi/10.1103/PhysRevLett.116.182502

[6] R. F. Garcia Ruiz, M. L. Bissell, K. Blaum et al., Unexpectedly large charge radii of neutron-rich calcium isotopes. Nature Physics. **12**, 594-598 (2016). doi.org/10.1038/nphys3645

[7] A. Koszorús, X. F. Yang, W. G. Jiang et al.,, Charge radii of exotic potassium isotopes challenge nuclear theory and the magic character of N = 32. Nature Physics. **17**, 439 (2021). doi.org/10.1038/s41567-020-01136-5

[8] B. Cheal,K. T. Flanagan, Progress in laser spectroscopy at radioactive ion beam facilities. Journal of Physics G: Nuclear and Particle Physics. **37**, 113101 (2010). doi.org/10.1088/0954-3899/37/11/113101

[9] P. Campbell, I.D. Moore, M.R. Pearson, Laser spectroscopy for nuclear structure physics. Progress in Particle and Nuclear Physics. **86**, 127 (2016). doi.org/10.1016/j.ppnp.2015.09.003

[10] E. Mané, J. Billowes, K. Blaum et al., An ion cooler-buncher for high-sensitivity collinear laser spectroscopy at ISOLDE. The European Physical Journal A. **42**, 503 (2009). doi:10.1140/epja/i2009-10828-0

[11] T.E. Cocolios, R.P. de Groote, J. Billowes et al., High-resolution laser spectroscopy with the Collinear Resonance Ionisation Spectroscopy (CRIS) experiment at CERN-ISOLDE. Nuclear Instruments and Methods in Physics Research Section B: Beam Interactions with Materials and Atoms. **376**, 284-287(2016). doi.org/10.1016/j.nimb.2015.11.024

[12] R. Neugart, J. Billowes, M. L. Bissell et al., Collinear laser spectroscopy at ISOLDE: new methods and highlights. Journal of Physics G: Nuclear and Particle Physics. **44**, 064002 (2017). doi:10.1088/1361-6471/aa6642

[13] R.P. de Groote, A. de Roubin, P. Campbell et al., Upgrades to the collinear laser spectroscopy experiment at the IGISOL. Nuclear Inst. and Methods in Physics Research B **463**, 437-440 (2020). doi.org/10.1016/j.nimb.2019.04.028

[14] A. Voss, T.J. Procter, O. Shelbaya et al., The Collinear Fast Beam laser Spectroscopy (Cfbs) experiment at Triumf. Nuclear Instruments and Methods in Physics Research Section A. **811**, 57 (2016). doi.org/10.1016/j.nima.2015.11.145

[15] K. Minamisono, P.F. Mantica, A. Klose et al., Commissioning of the collinear laser spectroscopy system in the BECOLA facility at NSCL. Nuclear Instruments and Methods in Physics Research Section A. **709**, 85 (2013). doi.org/10.1016/j.nima.2013.01.038

[16] D.T. Yordanov, D. Atanasov, M.L. Bissell et al., Instrumentation for high-resolution laser spectroscopy at the ALTO radioactive-beam facility. Journal of Instrumentation. **15**, P06004–P06004 (2020). doi:10.1088/1748-0221/15/06/p06004

[17] M. Reponen, R. P. de Groote1, L. Al Ayoubi et al., Evidence of a sudden increase in the nuclear size of proton-rich silver-96. Nature Communications. **12**, 4596 (2021). doi:10.1038/s41467-021-24888-x

[18] Annika Voss, Matthew R. Pearson, Jonathan Billowes et al., First Use of High-Frequency Intensity Modulation of Narrow-Linewidth Laser Light and Its Application in Determination of ^{206,205,204}Fr Ground-State Properties. Phys. Rev. Lett. **111**, 122501 (2013). doi:10.1103/PhysRevLett.111.122501

[19] A. J. Miller, K. Minamisono, A. Klose et al., Proton superfluidity and charge radii in proton-rich calcium isotopes. Nature Physics. **15**, 432-436 (2019). doi:10.1038/s41567-019-0416-9

[20] Y. Liu and Y. L. Ye, J. L. Lou et al., Positive-Parity Linear-Chain Molecular Band in ^{16}C. Phys. Rev. Lett. **124**, 192501 (2020). doi:10.1103/PhysRevLett.124.192501

[21] Y. B. Wang, J. Su, Z. Y. Han et al., Direct observation of the exotic $\beta - \gamma - \alpha$ decay mode in the $T_z = -1$ nucleus ^{20}Na. Phys. Rev. C **103**, L011301 (2021). doi:10.1103/PhysRevC.103.L011301

[22] Z. Y. Zhang, H. B Yang, M. H. Huang et al., New α-Emitting Isotope ^{214}U and Abnormal Enhancement of α-Particle Clustering in Lightest Uranium Isotopes. Phys. Rev. Lett. **126**, 152502 (2021). doi:10.1103/PhysRevLett.126.152502

[23] Y. Yang, L. T. Sun, Y. H. Zhai et al., Heavy ion accelerator facility front end design and commissioning. Phys. Rev. Accel. Beams **22**, 110101 (2019). doi:10.1103/PhysRevAccelBeams.22.110101

[24] Y. L. Ye., Proposed BISOL Facility - a Conceptual Design. EPJ Web Conf. **178**, 01005 (2018). doi:10.1051/epjconf/201817801005

[25] K. König, J. Krämer, C. Geppert et al., A new Collinear Apparatus for Laser Spectroscopy and Applied Science (COALA). Rev. Sci. Instrum. **91**, 081301 (2020). doi: 10.1063/5.0010903

[26] C Gorges, K Blaum, N Frömmgen et al., Isotope shift of ^{40,42,44,48}Ca in the 4s $^2S_{1/2} \rightarrow$ 4p $^2P_{3/2}$ transition. Journal of Physics B: Atomic, Molecular and Optical Physics. **48**, 245008 (2015). doi:10.1088/0953-4075/48/24/245008

[27] Patrick Müller, Kristian König, Phillip Imgram et al., Collinear laser spectroscopy of Ca$^+$: Solving the field-shift puzzle of the $4s^2\mathrm{S}_{1/2} \rightarrow 4p^2\mathrm{P}_{1/2,3/2}$ transitions. Phys. Rev. Research. **2**, 043351 (2020). doi:10.1103/PhysRevResearch.2.043351

[28] R.F. Garcia Ruiz, A.R. Vernon, C.L. Binnersley et al., High-Precision Multiphoton Ionization of Accelerated Laser-Ablated Species. Phys. Rev. X. **8**, 041005 (2018). doi:10.1103/PhysRevX.8.041005

[29] F. P. Gustafsson, C. M. Ricketts, M. L. Reitsma et al., Tin resonance-ionization schemes for atomic- and nuclear-structure studies. Phys. Rev. A. **102**, 052812 (2020). doi:10.1103/PhysRevA.102.052812

[30] A.R. Vernona, R.P. de Groote, J. Billowes et al., Optimising the Collinear Resonance Ionisation Spectroscopy (CRIS) experiment at CERN-ISOLDE. Nuclear Instruments and Methods in Physics Research Section B **463**, 384-389 (2020). doi.org/10.1016/j.nimb.2019.04.049

[31] K. Kreim, M.L. Bissell, J. Papuga et al., Nuclear charge radii of potassium isotopes beyond N=28. Physics Letters B. **731**, 97 (2014). doi.org/10.1016/j.physletb.2014.02.012

[32] Wouter Gins, Development of a dedicated laser-polarization beamline for ISOLDE-CERN. PhD thesis. 2019.

[33] S.W. Bai, Á. Koszorús, B.S. Hu, X.F. Yang, et al., Electromagnetic moments of scandium isotopes and N = 28 isotones in the distinctive $0f_{7/2}$ orbit, submitted (2021).

[34] Á. Koszorús, X. F. Yang, J. Billowes et al., Precision measurements of the charge radii of potassium isotopes. Phys. Rev. C. **100**, 034304 (2019). doi:10.1103/PhysRevC.100.034304